

# The climatological mean atmospheric transport under weakened Atlantic thermohaline circulation climate scenario

T. Erukhimova · R. Zhang · K. P. Bowman

Received: 25 August 2007 / Accepted: 24 March 2008 / Published online: 11 April 2008  
© Springer-Verlag 2008

**Abstract** Global atmospheric transport in a climate subject to a substantial weakening of the Atlantic thermohaline circulation (THC) is studied by using climatological Green's functions of the mass conservation equation for a conserved, passive tracer. Two sets of Green's functions for the perturbed climate and for the present climate are evaluated from 11-year atmospheric trajectory calculations, based on 3-D winds simulated by GFDL's newly developed global coupled ocean–atmosphere model (CM2.1). The Green's function analysis reveals pronounced effects of the climate change on the atmospheric transport, including seasonally modified Hadley circulation with a stronger Northern Hemisphere cell in DJF and a weaker Southern Hemisphere cell in JJA. A weakened THC is also found to enhance mass exchange rates through mixing barriers between the tropics and the two extratropical zones. The response in the tropics is not zonally symmetric. The 3-D Green's function analysis of the effect of THC weakening on transport in the tropical Pacific shows a modified Hadley cell in the eastern Pacific, confirming the results of our previous studies, and a weakening (strengthening) of the upward and eastward motion to the south (north) of the Equator in the western Pacific in the perturbed climate as compared to the present climate.

**Keywords** Climate change · Atmospheric transport · Atlantic thermohaline circulation · Green's function analysis · Hadley cell

## 1 Introduction

Global-scale atmospheric transport and circulation play a key role in determining the climate on our planet. Any change in the climate resulting from an imposed forcing will likely be manifested as changes in global transport patterns. Although many previous works have focused on climate change, they placed less emphasis on the response of atmospheric transport to various climate change scenarios. Studies of atmospheric transport are crucial in calculating distributions of minor constituents and contaminants; in understanding mass transfer, mixing barriers, and the connections between different areas in the atmosphere; and as a diagnostic tool for developing and improving general circulation models (GCMs). The paper is the first study of the atmospheric transport under abrupt climate change simulated by weakening of the Atlantic thermohaline circulation (THC).

Many recent theoretical and modeling studies show the potential for a slowing of the Atlantic Ocean's overturning circulation, resulting in changes in the atmospheric heat transport. Comparisons of five instantaneous surveys across 25°N since 1957 indicate a long-term slowdown of the THC (Bryden et al. 2005). Such observed snapshots might be aliased by observed large annual variations in the North Atlantic meridional heat flux. Several numerical experiments with coupled models have shown a weakened THC, cooling in the North Atlantic, warming in the South Atlantic, and the meridional shift of the intertropical convergence zone (ITCZ) in response to freshwater forcing in

---

T. Erukhimova (✉)  
Department of Physics, Texas A&M University,  
College Station, TX 77843-4242, USA  
e-mail: etanya@tamu.edu

R. Zhang  
GFDL/NOAA, Princeton, NJ, USA

K. P. Bowman  
Department of Atmospheric Sciences,  
Texas A&M University, College Station, TX, USA

the North Atlantic (e.g., Vellinga and Wood 2002; Chiang 2003; Dahl et al. 2005; Stouffer et al. 2006; Broccoli et al. 2006; Cheng 2007; Timmermann et al. 2005, 2007). Zhang and Delworth (2005) used a coupled ocean–atmosphere model to show that a steady freshwater forcing in the North Atlantic weakens the Atlantic THC resulting in global-scale changes in the tropics: a southward shift of ITCZ over the Atlantic and Pacific, an El Niño-like pattern in the southeastern tropical Pacific and weakened Indian and Asian summer monsoons. These changes are consistent with abrupt climate changes indicated by paleoclimate records (Peterson et al. 2000; Wang et al. 2001, Altabet et al. 2002; Koutavas et al. 2002, Wang et al. 2004).

In this study, global-scale velocity fields obtained from the latest fully coupled ocean–atmosphere global general circulation model, version CM2.1, developed at the Geophysical Fluid Dynamics Laboratory, are used for calculations of the Lagrangian trajectories of massless air parcels in order to study transport properties of the flow under the abrupt (substantially weakened THC) climate change scenario. Lagrangian methods have proven to be very useful in understanding transport problems in the atmosphere (Hsu 1980; Matsuno 1980; Kida 1983; Austin and Tuck 1985; Schoeberl et al. 1992; Bowman 1993; Pierce and Fairlie 1993; Pierrehumbert and Yang 1993; Chen 1994; Sutton et al. 1994; Bowman 1996; Bowman and Carrie 2002; Bowman and Erukhimova 2004; Erukhimova and Bowman 2006). A comparison between the climatological transport patterns following an abrupt climate change (referred to as the Perturbed case) and an unperturbed case (referred to as the Control case) is done in terms of Green’s functions. The Green’s functions of the transport equation were used in previous studies by Hall and Plumb (1994), Holzer (1999), and Holzer and Hall (2000). Holzer and Boer (2001) applied the Green’s function method to study the changed trace gas distributions under the global warming by online integration of the continuity equation for a passive tracer.

In Bowman and Erukhimova (2004) we estimated the climatological Green’s functions for the mass conservation equation for a conserved, passive tracer under the present climate scenario. It was found that in terms of the transport of trace species, the atmosphere is divided into three major zones: the tropics, and the two extratropics zones in the Northern and Southern Hemispheres. Transport within each of these zones is relatively fast, while the exchange of air between the zones is relatively slow due to the existence of semi-permeable “barriers”. The interhemispheric transport rates calculated using the Green’s functions agreed well with measurements of long-lived trace species from atmospheric lifetime experiment/global atmospheric gases experiment (ALE/GAGE) network. Taking into account convection (Erukhimova and Bowman 2006) does

not change the transport pattern qualitatively, although it can lead to a significant local changes in the transport.

Following Bowman and Carrie (2002), Bowman and Erukhimova (2004), and Erukhimova and Bowman (2006), we estimate the climatological Green’s functions from a large ensemble of long-term Lagrangian trajectories calculated under the Perturbed and Control case climate scenarios, respectively.

Zhang and Delworth (2005) found a significant change in the tropical atmospheric deep convection and atmospheric mass transport in the abrupt climate change scenario (Perturbed case): an anomalous cross-equator annual mean Hadley circulation is developed in response to the weakening of the Atlantic THC, with rising motion south of the Equator and descending motion north of the Equator. This is consistent with a southward shift of the ITCZ and enhanced northward atmospheric heat transport across the Equator. Our study here extends the work by Zhang and Delworth (2005) in several different directions. First, the trajectory analysis allows one to follow air parcels released at a particular point and find their distribution after any specified time. In particular, we investigate the effect of an abrupt climate change on the interhemispheric transport and mixing barriers between the tropics and the two extratropical zones. Second, we study seasonal variations of the 3D atmospheric transport in the Perturbed and Control cases by comparing the results for two solstitial seasons, DJF and JJA. Third, we investigate and verify the changes in the 3-D transport circulation in the tropical Pacific suggested by the anomalous precipitation and vertical velocity patterns obtained by Zhang and Delworth (2005).

## 2 Description of models and method

### 2.1 Global general circulation model

The global general circulation model used in this study is the latest fully coupled ocean-atmosphere model (CM2.1) developed at the Geophysical Fluid Dynamics Laboratory (GFDL). The ocean model employs an explicit free surface and a true freshwater flux exchange between the ocean and the atmosphere. It has 50 vertical levels (22 levels of 10-m thickness each in the top 220 m) and 1° zonal resolution. The meridional resolution is 1° outside the tropics, refined to 1/3° at the Equator. The atmosphere model has 24 vertical levels, with horizontal resolution of 2° latitude × 2.5° longitude. The model uses radiative forcing for the year 1860 and produces a stable, realistic, multicentury control integration without flux adjustments (Delworth et al. 2006).

To explore the climate change induced by a weakening of the Atlantic THC, a perturbation experiment is

conducted in which extra freshwater forcing of 0.6 Sv (1Sv = 10<sup>6</sup> m<sup>3</sup>s<sup>-1</sup>) is uniformly distributed over the northern North Atlantic (55°–75°N, 63°W–4°E) for the entire 60-year duration of the experiment. The fresh water forcing is introduced at each time step. The amplitude of the forcing is relatively large in order to elicit a clear response. The design of this experiment is the same as that described in Zhang and Delworth (2005). In the perturbed experiment, the maximum Atlantic THC rapidly weakens from 23 Sv (time mean in the control run of CM2.1) to about 7 Sv after 20 year, after which the rate of decrease gradually slows, resulting in an average of 4 Sv from years 21 to 60. The analyses in this paper are focused on the differences between the two experiments (Perturbed and Control cases) averaged over years 43–53, during which time the weakened THC has stabilized to an average of 3 Sv for this period. Three-dimensional atmospheric velocities are archived every 6 h and used as input for the trajectory model.

### 2.2 Trajectory model and Green’s function method

The transport circulation is estimated using the ensemble-mean Green’s functions (Bowman and Carrie 2002; Bowman and Erukhimova 2004; Erukhimova and Bowman 2006). This technique is a computationally economical way to provide a quantitative description of the climatological transport of a conserved passive tracer from an arbitrary initial location  $x_0$ . If the initial mass mixing ratio of a conserved passive tracer,  $\chi_0$ , is known, the ensemble-mean tracer distribution at future times can be found from the ensemble-mean Green’s function  $\langle G(\mathbf{x}, \mathbf{x}_0, t) \rangle$  (Bowman and Carrie 2002):

$$\langle \chi(\mathbf{x}, t) \rangle = \int_{\mathbf{x}_0} \chi_0(\mathbf{x}_0) \langle G(\mathbf{x}, \mathbf{x}_0, t) \rangle d\mathbf{x}_0, \tag{1}$$

where  $\mathbf{x}$  is position,  $t$  is time,  $\chi$  is the mass mixing ratio of the tracer, index 0 is for the initial time moment, brackets indicate ensemble-mean solution.

The Green’s functions are estimated from particle trajectories. Particle trajectories are described by the equation

$$\frac{d\mathbf{x}'}{dt} = \mathbf{v}(\mathbf{x}', t), \quad \mathbf{x}'(t_0) = \mathbf{x}_0' \tag{2}$$

where  $\mathbf{x}'$  is the position of the particle as a function of time  $t$ , and  $\mathbf{x}_0'$  is the initial location of the particle at  $t = t_0$ . The velocity  $\mathbf{v}$  in the right-hand side of (2) is a large-scale velocity, which is taken from the CM2.1 calculations.

We assume that tracer’s mass mixing ratio obeys the purely advective mass continuity equation:

$$\frac{\partial \chi}{\partial t} + \mathbf{v} \cdot \nabla \chi = 0, \quad \chi(\mathbf{x}, t_0) = \chi_0(\mathbf{x}), \tag{3}$$

Because the trajectories are the characteristics of the purely advective mass continuity equation for a conserved tracer, the Green’s function for (3) can be written as

$$G(\mathbf{x}, \mathbf{x}_0, t) = \delta(\mathbf{x} - \mathbf{x}'(\mathbf{x}_0', t)), \tag{4}$$

where  $\mathbf{x}_0 = \mathbf{x}_0'$  and  $\mathbf{x}'(\mathbf{x}_0', t)$  is the solution to the trajectory equation (2).

In practice the Green’s function is not defined everywhere. Here we estimate discrete (gridded) Green’s functions  $G(\mathbf{x}, \mathbf{x}_0, \delta t)$ , where  $\mathbf{x}_0$  is the initial location,  $\mathbf{x}$  is the final location, and  $\delta t$  is the time elapsed since the ensemble of parcels left the initial location. A discrete approximation to the Green’s function can be estimated by computing the discrete probability density function of the parcels (Bowman and Carrie 2002)

$$\langle G_i(\mathbf{x}, \mathbf{x}_0, \delta t) \rangle \Delta V_i = \frac{\langle m_i(\mathbf{x}_0, t) \rangle}{N}, \tag{5}$$

where  $m_i$  is the number of  $\delta$  functions initially in the grid box  $\Delta V_0$  at  $\mathbf{x}_0$  at time  $t_0$  that are in the grid box  $\Delta V_i$  at  $\mathbf{x}_i$  at time  $t$ ,  $N$  is the number of parcels. The discrete probability density function of parcels is computed by dividing the domain into a regular, 3-D array of grid boxes. The number of parcels in each grid box gives a distribution of parcels initially at  $\mathbf{x}_0$  at time  $t_0$  that are in grid box  $i$  at time  $t$ .

The ensemble-mean Green’s functions in (1) are calculated by averaging over different initial times within a month. These are then averaged together to compute seasonal or climatological means. The time averages for this study cover 11 years. Due to the large number of parcels used, the sampling errors arising from estimating  $\langle G \rangle$  by counting parcels are generally small (Bowman and Carrie 2002).

The trajectories are calculated by solving equation (2) numerically. Standard fourth-order Runge–Kutta scheme with 32 time steps per day is used. Velocities at arbitrary  $\mathbf{x}'$  and  $t$  are computed by linear interpolation in space and time.

There are several reasons to use a purely advective approach for this study. We calculate air parcel motion using only the resolved large-scale winds, neglecting molecular diffusion and small-scale, unresolved components of the velocity field. The unresolved velocity components are, by definition, unknown. Including them would require making major assumptions about their characteristics. Moreover, observational and theoretical studies indicate that the atmospheric energy spectrum falls off with decreasing spatial scale, so the smaller scales do not contribute substantially to the global-scale transport on

the time scales of interest here. It should be also noted that the qualitative effect of unresolved scales would likely be to smear out a localized initial tracer distribution. In this study, however, we analyze the ensemble-mean transport characteristics by averaging over many different flow fields. It seems to be a reasonable assumption that the smearing due to variability in the resolved flow dominates any contribution from the unresolved flow.

We neglect the convective transport that could enhance the vertical dispersion of air parcels. However, as was shown in Erukhimova and Bowman (2006), including the effect of convection can lead to significant local differences in the distribution of a passive tracer but does not change the global transport picture qualitatively. Future studies are necessary to understand the effect of convection on the tracer distribution in the Perturbed case.

### 3 Results

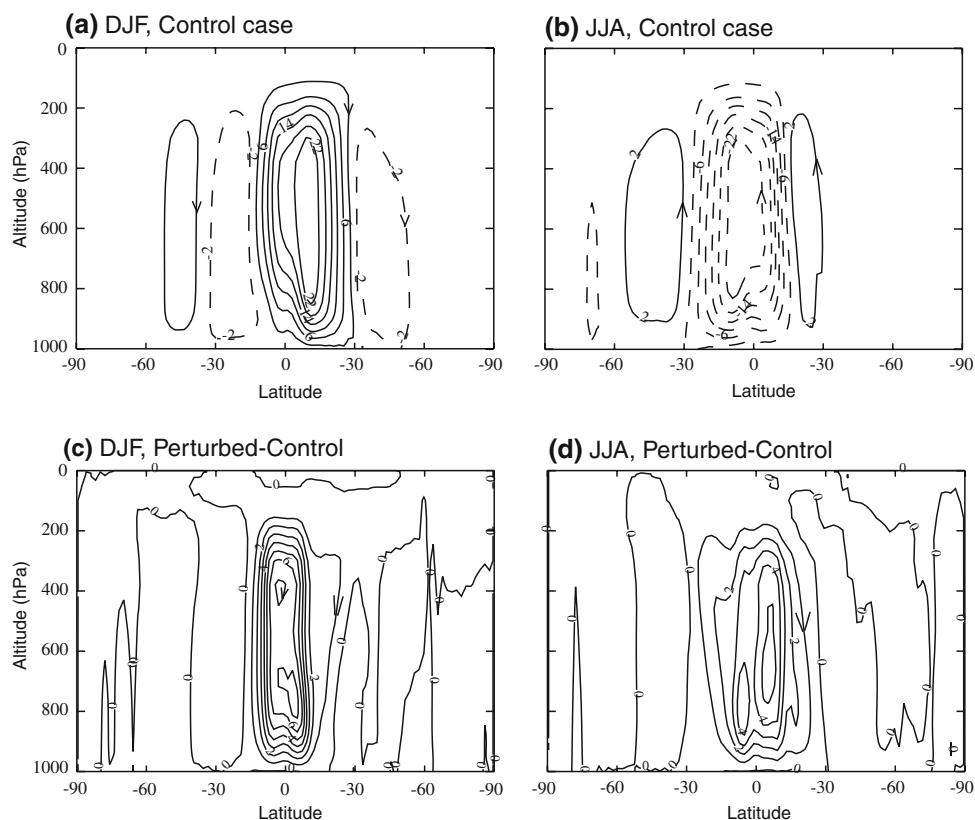
In this paper we focus on differences in the climatological atmospheric transport circulation for the solstitial seasons, December–February (DJF) and June–August (JJA). Zonally averaged and 3-D Green’s functions (Bowman 2006) are analyzed to find out how the transport properties change in the Perturbed case (abrupt climate change scenario). In order that individual parcels approximately

represent equal masses of air, trajectories are randomly initialized in longitude, sine of latitude, and pressure. A total of  $N = 4 \times 10^5$  parcels trajectories are integrated continuously for 11 years of experiment.

#### 3.1 2-D transport in the latitude-altitude plane

The top panels (a) and (b) of Fig. 1 show the climatological zonal-mean mass stream functions for DJF and JJA for the Control case. The climatological mean Hadley circulation in the present climate has a strong winter-hemisphere cell and a very weak summer-hemisphere cell during both solstitial seasons. During DJF the dominant winter (Northern Hemisphere) cell has a clockwise circulation with northward atmospheric heat transport. During JJA the winter (Southern Hemisphere) cell has a counterclockwise circulation with southward atmospheric heat transport. The bottom panels (c) and (d) show the differences between the zonal mean mass stream functions for the Perturbed and Control cases. The circulation anomaly induced by the weakening of the Atlantic THC strengthens the dominant Hadley cell and northward heat transport during DJF, and weakens the dominant cell during JJA. Such a change in the Hadley circulation is induced by the North Atlantic cooling/South Atlantic warming and the reduced northward ocean heat transport associated with the substantially weakened Atlantic THC (Zhang and Delworth 2005). This

**Fig. 1** Seasonal mean zonally integrated atmosphere stream function for the Control case and stream function anomaly (Perturbed–Control); all in  $10^{10}$  kg/s. DJF period (a, c); JJA period (b, d)



results in a southward shift of the ITCZ and an enhanced northward atmospheric heat transport across the Equator in the Perturbed case compared to the Control case.

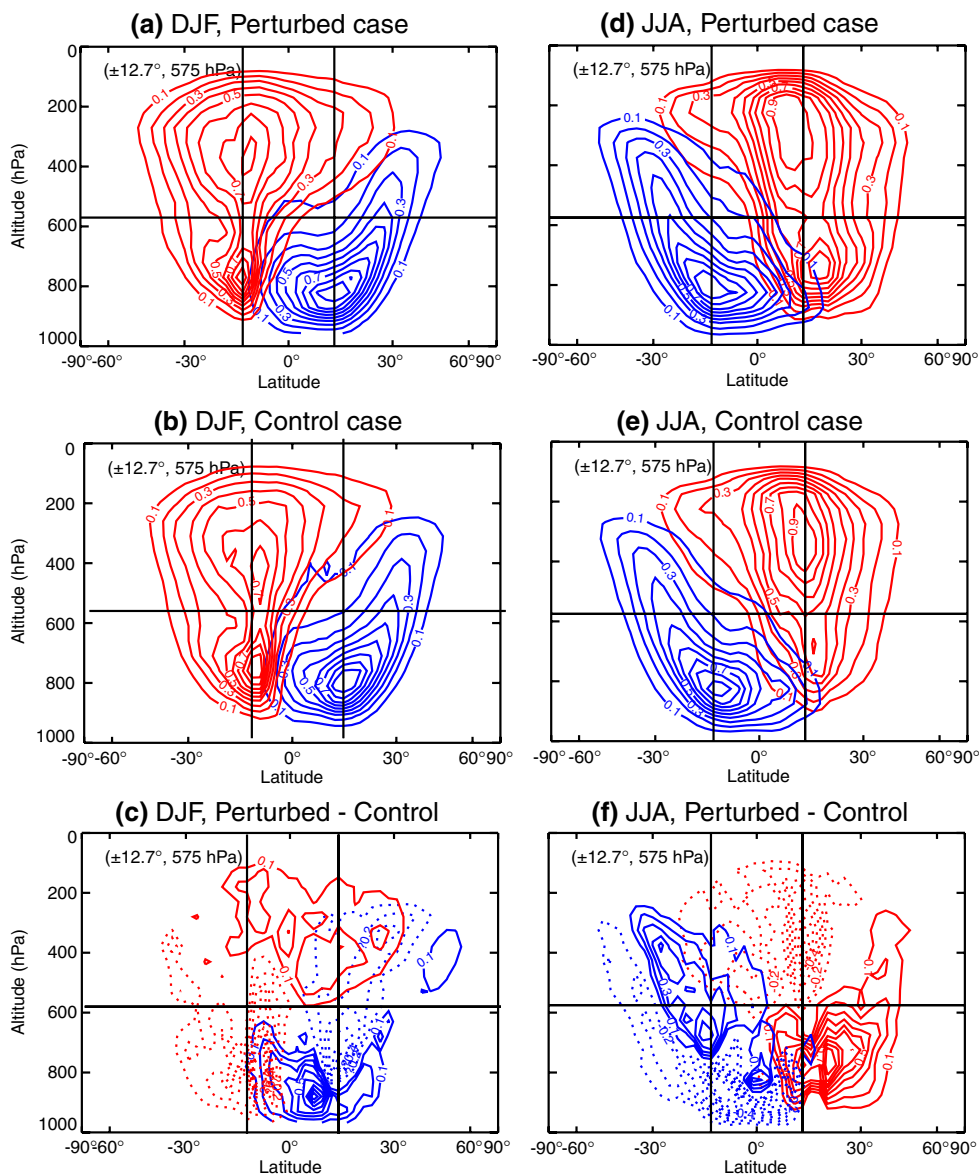
The strengthening of the dominant Hadley cell in DJF and its weakening in JJA in the Perturbed case as compared to the Control case climate scenario lead to a strong relative seasonal change in the Lagrangian trajectories. Figure 2 shows the transport circulations in the tropics for DJF and JJA. The distribution is plotted 10 days after the parcels' initial release at ( $\pm 12.7^\circ, 575$  hPa). For more direct comparison we plot the differences between distributions in the Perturbed and Control cases (Fig. 2c, f). The differences are normalized by the number of parcels at the initial location since it could be different for Perturbed and Control cases. For example, if  $n_1(0)$  and  $n_2(0)$  are the numbers of parcels at a given initial location at the initial

time, and  $n_1$  and  $n_2$  are the numbers of parcels at the destination location at the time of interest, then the normalized difference (NDIF) is

$$\text{NDIF} = \frac{n_1}{n_1(0)} - \frac{n_2}{n_2(0)}. \tag{6}$$

Here index 1 corresponds to the Perturbed case, and index 2 corresponds to the Control case. To find the relative difference between the Perturbed and Control cases with respect to Control case, NDIF is divided by  $n_2/n_2(0)$ . If the initial number of parcels is the same for the two cases, ( $n_1(0) = n_2(0)$ ), then  $\text{NDIF}/n_2 = (n_1 - n_2)/n_2$ . During DJF (Fig. 2c) more parcels descend in the Northern Hemisphere (solid blue contours) and rise in the Southern Hemisphere (solid red contours) in the Perturbed climate scenario as compared to the Control simulation. In JJA the circulation

**Fig. 2** Climatological Green's functions and normalized differences for 10 days after parcels are initially released in the tropical middle troposphere for the Perturbed and Control cases. DJF period (*left*). JJA period (*right*). The abscissa is the sine of the latitude. Two initial conditions, symmetric about the Equator, are shown in each panel. The initial conditions are indicated by a label and the intersecting lines. The contours indicate the parcel density at the given time, normalized by the maximum value. [Red contours are for the parcels released in the summer hemisphere; blue contours are for the parcels released in the winter hemisphere; solid (dashed) lines correspond to positive (negative) values of Perturbed–control (c, f)]



anomaly has the same sense (Fig. 2f): more parcels descend in the Northern Hemisphere (solid red contours) and rise in the Southern Hemisphere (solid blue contours) in the Perturbed case compared to the Control case. The maximum relative differences between Perturbed and Control cases with respect to Control case are  $\sim 70\%$  for DJF and  $\sim 80\%$  for JJA. Of course, such large changes are reached locally. Note that in the ascending branch of the Hadley circulation the majority of air parcels rise, but a substantial number of parcels actually descend. This is to be expected in a convective circulation that has both rising and sinking motion.

In the extratropics, parcels disperse rapidly along isentropes due to eddies, but move more slowly across the isentropes due to diabatic effects. Exchange of air with the

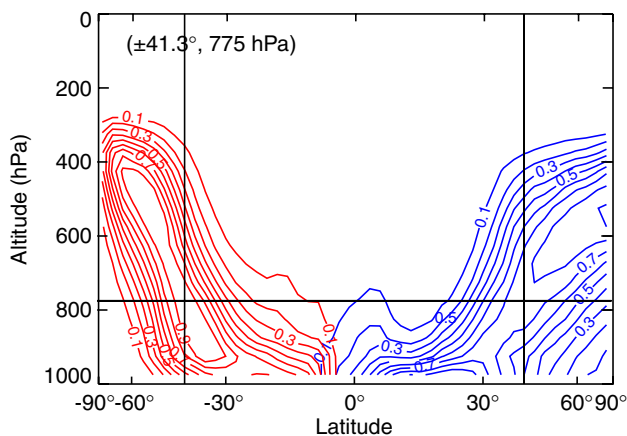


**Fig. 3** Green's functions calculated for parcels released in the extratropical lower troposphere ( $\pm 41.3^\circ$ , 775 hPa) in DJF period in the Perturbed case for the period of 10 days after their initial release. The abscissa is the sine of the latitude. The *intersecting lines* indicate the initial parcel positions. (Red summer hemisphere; blue winter hemisphere)

tropics is slow due to the existence of partial transport barriers located near  $30^\circ$  in both hemispheres, sloping upward toward the poles. This is true for both solstitial seasons (see Bowman and Erukhimova 2004; Erukhimova and Bowman 2006). As an example, we show the dispersion of parcels released in the extratropical lower troposphere at ( $\pm 41.3^\circ$ , 775 hPa) in DJF in the Perturbed case (see Fig. 3). The values are plotted for 10 days after the initial release of the parcels. Partial barriers exist in both the Perturbed and Control cases. However, there are quantitative differences between the cross-isentropic parcel dispersion for the two cases. Figure 4 shows the normalized differences between the Perturbed and Control cases for DJF and JJA 10 days after the parcels initial release. There is a pronounced motion across the isentropes from the point of particles release in the extratropics toward the equatorial region below 800 hPa. One can conclude that the transport barriers are less pronounced in the Perturbed case than in the Control case.

The differences between the transport circulations under the two climate scenarios for DJF and JJA are shown in Fig. 5. The net (Perturbed–Control) most probable transport path (the difference of the displacements of the peak of the parcel distribution from its initial location for each scenario) is shown after 7.5 days for a large grid of initial conditions. The most pronounced difference in parcel distributions between the Perturbed and Control cases is in the tropics: more parcels ascend in the Southern Hemisphere and sink in the Northern Hemisphere for both seasons in the Perturbed case as compared to the Control case climate scenario. In the extratropics, there is stronger rising motion in the Southern Hemisphere and descending motion in the Northern Hemisphere in the Perturbed case compared to the Control case in JJA. The motion is approximately along the isentropes. In DJF the pattern is more chaotic with no

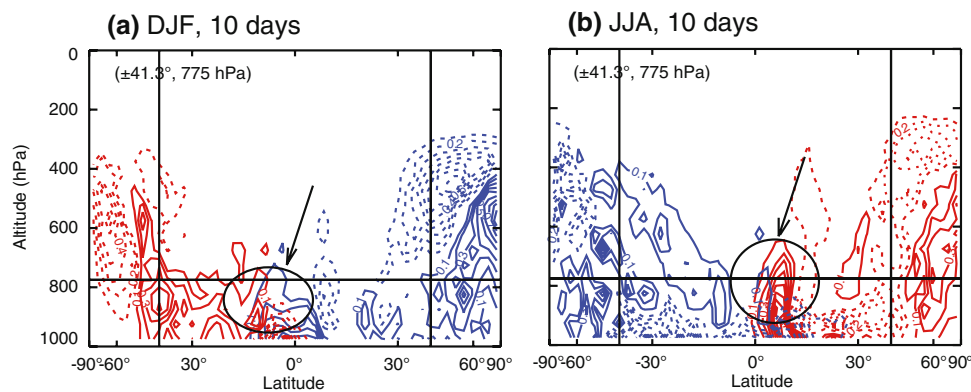


**Fig. 4** Normalized differences between Perturbed and Control cases for parcels released at ( $\pm 41.3^\circ$ , 775 hPa): DJF period (a); JJA period (b) after 10 days. The abscissa is the sine of the latitude. The *intersecting lines* indicate the initial parcel positions. (Red summer

hemisphere; blue winter hemisphere.) *Solid (dashed) lines* correspond to positive (*negative*) values of Perturbed–Control. *Black arrows and circles* indicate the parcels resulting from the enhanced motion across the barriers

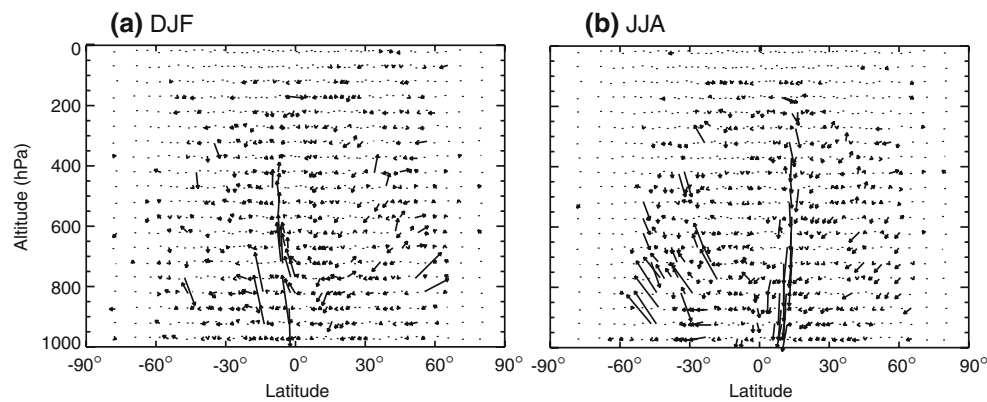


**Fig. 5** The differences between the most probable parcels motion between Perturbed and Control cases in the altitude–latitude plane. The differences are calculated as a function of initial position of the

clear difference between the motion along and across the isentropes.

To make a quantitative comparison of transport across the transport barriers between the Perturbed and Control cases, we adopt the simple 3-box model previously used in Bowman and Carrie (2002), Bowman and Erukhimova (2004), and Erukhimova and Bowman (2006). The model divides the entire atmosphere into three boxes: the Southern Hemisphere extratropics (90°S–30°S), the Northern Hemisphere extratropics (30°N–90°N), and the tropics (30°S–30°N), which contains twice as much air as the extratropical boxes. With this crude approximation, it is assumed that the tropical region exchanges air with both extratropical boxes at equal and constant rate  $r$ . The mass conservation equations for each box are

$$\begin{aligned} \frac{d\chi_S}{dt} &= -r\chi_S + r\chi_T, \\ \frac{d\chi_T}{dt} &= \frac{1}{2}r\chi_S - r\chi_T + \frac{1}{2}r\chi_N, \\ \frac{d\chi_N}{dt} &= +r\chi_T - r\chi_N \end{aligned} \quad (7)$$

where  $\chi_S$ ,  $\chi_T$ , and  $\chi_N$  are the mass mixing ratios of the tracer in the Southern Hemisphere, tropical, and Northern Hemisphere boxes, respectively; and  $r$  is the rate of mass exchange between the boxes relative to the mass of an extratropical box.

We assume that a tracer is initially within the Northern Hemisphere box:  $\chi_S = 0$ ,  $\chi_T = 0$ ,  $\chi_N = 4$ . From (7), the time dependent solutions for the concentrations in each box are:

$$\begin{aligned} \chi_S(t) &= 1 - 2 \exp(-rt) + \exp(-2rt) \\ \chi_T(t) &= 1 - \exp(-2rt), \\ \chi_N(t) &= 1 + 2 \exp(-rt) + \exp(-2rt) \end{aligned} \quad (8)$$

At short times, the concentrations grow or decay exponentially with time scales  $1/r$  or  $1/2r$  as the tracer mixes

parcels. The *arrows* indicate the the displacement (Perturbed–Control) after 7.5 days of the peak of the zonal-mean probability distribution from each initial location

from the Northern Hemisphere box into the tropical and the Southern Hemisphere box. As  $t \rightarrow \infty$ , the tracer becomes uniformly mixed throughout the three boxes with a concentration of 1.

The temporal distribution of the tracer is estimated from the Green’s functions. For comparison with the box model the tracer is initially uniformly distributed between 45 and 90°N and 1,000 and 300 hPa for the Perturbed and Control experiments. The upper boundary at 300 hPa is chosen to ensure that the tracer is initially contained entirely in the Northern Hemisphere troposphere. Then, the mass exchange coefficient  $r$  was estimated by fitting the data with analytical expressions of the form given by the solution of (8). Fitting separately to each of the three curves gives somewhat different values of the mass exchange rate between the boxes,  $r$ . This difference could be meaningful, indicating that we should have used different exchange rates for the Northern and Southern Hemispheres. However, we do not pursue it here, concentrating instead on the differences between the Perturbed and Control cases.

The exchange rate  $r$  can be expressed in terms of the time lag between hemispheres for a constant source in the Northern Hemisphere. The source term is included in the right-hand side of the mass conservation equation for the Northern Hemisphere (see Bowman and Carrie 2002 for details).

The results for the mass exchange rate and the lag in concentrations between the Northern Hemisphere and Southern Hemisphere for the Perturbed and Control cases are summarized in Table 1. For both climate scenarios, the mass exchange rate between the hemispheres is slightly but persistently larger for the DJF period as compared to the JJA period. This result is in agreement with our previous studies with a GCM for the present climate (Bowman and Erukhimova 2004; Erukhimova and Bowman 2006). The mass exchange rates estimated from NCEP reanalysis do not show such tendency between the seasons (see Bowman

**Table 1** Top two rows: mass exchange rate between the boxes as a percentage of the mass in one of the extratropical boxes (25% of the total atmosphere)

	DJF			JJA		
	NH	Tropics	SH	NH	Tropics	SH
Mass exchange rate (% per day)						
Control	1.22	1.43	0.76	0.82	0.91	0.63
Perturbed	1.37	1.57	0.88	0.89	0.99	0.67
NH → SH tracer lag for constant source (years)						
Control	0.90	0.77	1.43	1.33	1.21	1.73
Perturbed	0.78	0.70	1.25	1.23	1.10	1.65

The three estimates for each region [Northern Hemisphere (NH), Tropics, and Southern Hemisphere (SH)] use the time history of the tracer concentration in the respective box. Bottom two rows: lag of the concentration of a conserved passive tracer in the Southern Hemisphere extratropics relative to the Northern Hemisphere extratropics

and Erukhimova 2004). The reason for such disagreement may be because of the crudeness of the 3-box model, where we assume that the boundaries between the boxes are vertical rather than sloping, and that the exchange rate between the hemispheres is constant.

As Table 1 shows, the mass exchange rates between the tropics and extratropics, and between the hemispheres, are consistently slightly larger in the Perturbed Case than in the Control Case for both seasons. This agrees with the results in Fig. 4, which shows that the barriers are weaker in the Perturbed Case on short time scales. The dynamical mechanisms responsible for the existence of semipermeable transport barriers between the tropics and extratropics are not fully understood at this time, but clearly involve the latitudinal transition between the eddy-dominated circulation of the extratropics and the convective regime of the tropical Hadley circulation. A detailed analysis of the mechanisms responsible for the changes in transport rates is reserved for future study.

### 3.2 3-D transport in the tropical Pacific

The mechanism of remote responses in the tropical Pacific was pointed out in Zhang and Delworth (2005). The link is through the central American region with strong cooling in the tropical Atlantic off the central American coast. This cooling leads to a sea level pressure anomaly and sea surface temperature (SST) dipole anomaly (averaged difference Perturbed-Control) across the eastern tropical Pacific with cooling north of the Equator and warming in the cold tongue south of the Equator. This cooling enhances sea-level pressure (SLP) in the eastern tropical Pacific off the Central American coast, which induces anomalous southward surface winds across the Equator in the eastern

Pacific. The SST dipole anomaly across the eastern tropical Pacific further amplifies the anomalous southward wind flow, moisture transport, ITCZ shift, and the anomalous Hadley circulation. As a result, the southeast trade wind and thus the Walker circulation south of the Equator are weakened while the northeast trade wind and thus the Walker circulation north of the Equator are enhanced.

Since the response in the tropical Pacific to the weakening of the Atlantic THC is not zonally symmetric, we use 3-D Green's functions to find out the changes in the atmospheric transport circulation. In this paper we concentrate on the two important effects: the anomalous transport in the eastern tropical Pacific triggered by the modified Hadley cell and the altered east-west transport with different sign south and north of the Equator.

Figures 6 and 7 show the climatological dispersion of parcels released at 950 hPa height in the eastern tropical Pacific at 115°W to the north and south of the Equator in the Perturbed and Control cases. All distributions are plotted for DJF season. After 7 days there is stronger upward motion south of the Equator in the Perturbed case than in the Control case (see Fig. 6a, b). The situation is the opposite north of the Equator (Fig. 7a, b): parcels are dispersed weaker upwards and eastward in the Perturbed case than in the Control case. This happens because of the strengthening of the Hadley cell and southward shift of the ITCZ over the eastern tropical Pacific in the Perturbed case as a response to the weakening of THC. Following the 3-D motion of the parcels in time, we see that the parcels released in the eastern Pacific north of the Equator propagate upwards rather than across the Equator, although there are strong cross-equator southward winds in the eastern Pacific as a result of the weakened THC. Over a longer period of 15 days (Figs. 6, 7c, d), one can see the dynamics in the zonal direction: stronger (weaker) eastward transport at upper level for the parcels released south (north) of the Equator in the Perturbed case than in the Control case, consistent with the changes in Hadley circulation.

The western tropical Pacific response to the weakening of the Atlantic THC is shown in Fig. 8 where all distributions are for DJF season at 950 hPa level, 20 days after the initial release of the parcels. For parcels released in the northwestern tropical Pacific at 135°E, 12°N, there is stronger upward and then eastward transport in upper levels (Fig. 8a) in the Perturbed case in comparison with the Control case (Fig. 8b); the upward and eastward transport of the parcels released in the southwestern tropical Pacific at 155°E, 12°S is weaker in the Perturbed case than that in the Control case (see Fig. 8c, d for the Perturbed and Control cases, respectively). The differences between the two cases to the south and north of the Equator are consistent with vertical velocity and precipitation anomalies found by Zhang and Delworth (2005) (their Figs. 1d, 2a) indicating

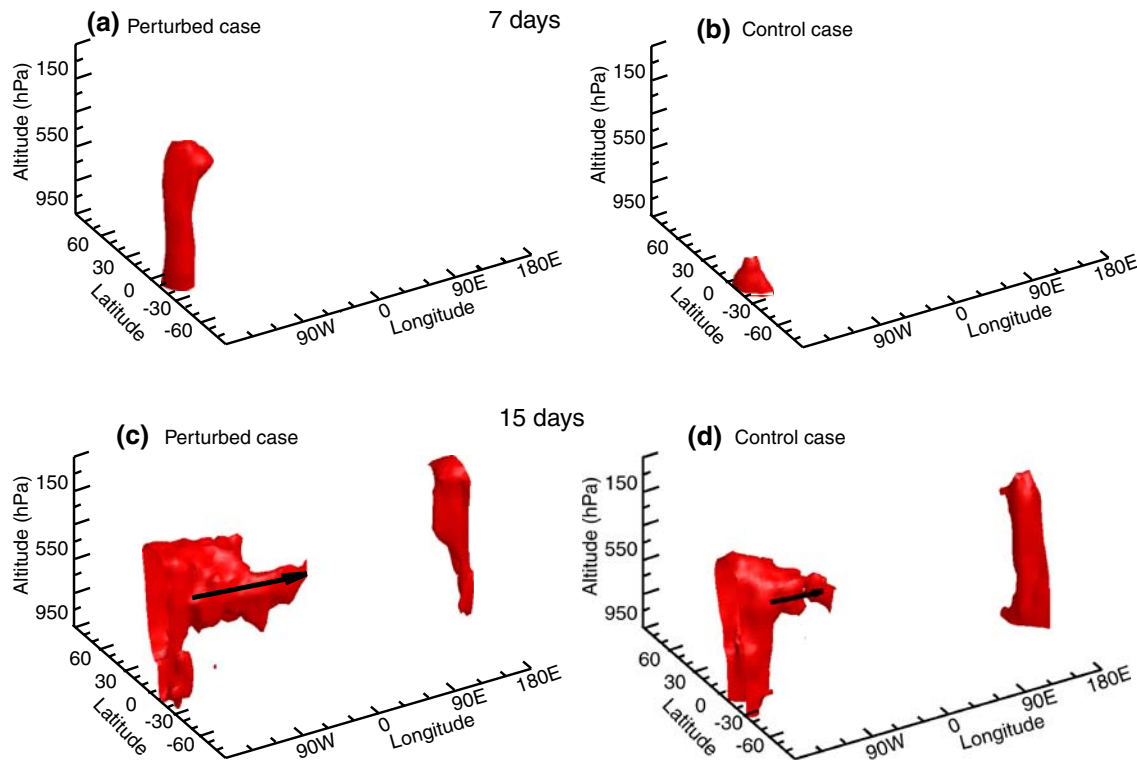


**Fig. 6** 3-D Green's functions calculated for the parcels released at 12°S, 115°W, 950 hPa, for DJF period. Perturbed case (*left panel*); Control case (*right panel*). Distributions are plotted for 7 days (**a, b**) and 15 days (**c, d**) after parcels' initial release. (See Sect. 3.1 for details)

an “El Niño-like” pattern (weakened Walker circulation) south of the Equator and a “La Niña-like” pattern (strengthened Walker circulation) north of the Equator (the terms “El Niño-like” and “La Niña-like” point to the analogy to the spatial pattern of El Niño and La Niña).

#### 4 Conclusions

Green's functions calculated from 11 years of Lagrangian trajectory simulations reveal pronounced changes in transport in a climate subjected to weakening of the thermohaline circulation. The substantial weakening of the THC, accompanied by North Atlantic cooling/South Atlantic warming, reduced northward ocean heat transport, a southward shift of the ITCZ, and enhanced northward atmospheric heat transport, strengthens the winter-hemisphere Hadley cell in DJF and weakens it in JJA in the Perturbed case compared to the Control case. The transport circulation anomaly (Perturbed–Control) is similar for the two solstitial seasons. It is dominated by a single cell with rising motion south of the Equator and sinking motion north of the Equator. Its structure resembles the total circulation for DJF. The maximum relative differences between the Perturbed and Control cases are up to 70–80%

for both seasons (reached locally at the peaks of the distributions, Fig. 2e, f).

In the extratropics the transport circulation is similar in the Perturbed and Control cases: there are transport barriers between tropics and extratropics located around  $\pm 30^\circ$  that tilt poleward. However, the barriers are less pronounced in the Perturbed case, making the mass exchange rate between the tropics and extratropics slightly but persistently larger.

The freshwater forcing in the North Atlantic causes a remote response in the tropical Pacific. The strengthened Hadley cell during DJF and the southward shift of the ITCZ in the Perturbed case result in stronger upward and eastward motion of the parcels released in the eastern Pacific at 115°W south of the Equator. For parcels released north of the Equator at the same longitude there is stronger upward and eastward transport in the Control case as compared to the Perturbed case.

The 3-D transport circulation in the western tropical Pacific shows the stronger (weaker) upward and eastward motion for the parcels released to the north (south) of the Equator in the Perturbed case as compared to the Control case. This effect is consistent with the reduced east-west SST contrast in the southeastern Pacific and the southward ITCZ shift over the eastern tropical Pacific observed in the simulations by Zhang and Delworth (2005). According to

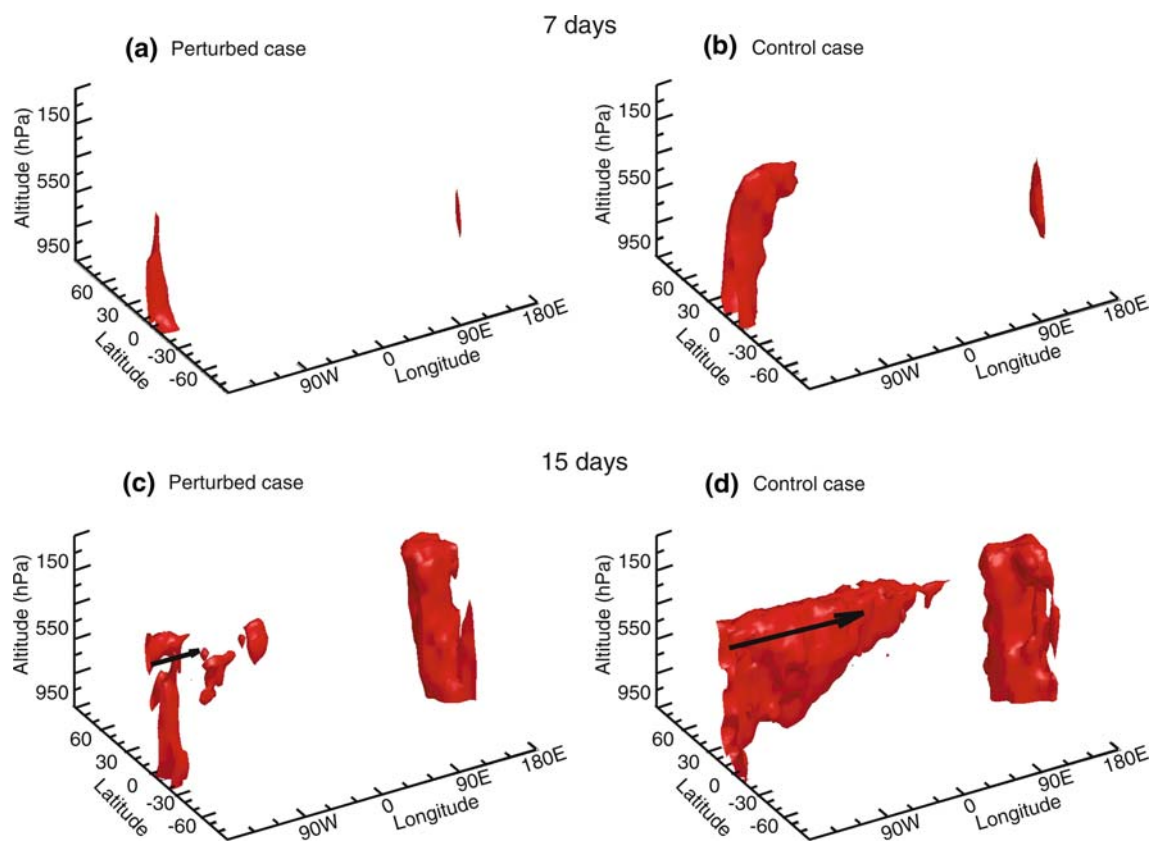


**Fig. 7** 3-D Green's functions calculated for the parcels released at 12°N, 115°W, 950 hPa for DJF period. Perturbed case (*left panel*); Control case (*right panel*). Distributions are plotted for 7 days (**a**, **b**) and 15 days (**c**, **d**) after parcels' initial release. (See Sect. 3.1 for details)

their work, the mechanism of response with different sign north and south of the Equator in the tropical Pacific is associated with the atmospheric response to the weakened Atlantic THC, i.e., the anomalous Hadley circulation across the equator. The substantially weakened Atlantic THC causes the changes in the Eastern Pacific through the central American region: enhanced SLP in the eastern tropical Pacific off the Central American coast, anomalous southward surface winds across the equator in the eastern Pacific, and, as a result, anomalous ocean upwelling and thus cooling in the eastern tropical Pacific north of the Equator, and anomalous ocean downwelling and thus warming in the cold tongue south of the Equator. The SST dipole anomaly across the eastern tropical Pacific further amplifies the anomalous southward wind flow, moisture transport, ITCZ shift, and the anomalous Hadley circulation. Hence the southeast trade wind and thus the Walker circulation south of the equator are weakened, and the upwelling in the southeastern Pacific is further weakened. The northeast trade wind and thus the Walker circulation north of the equator are enhanced, and the upwelling in the northeastern Pacific is further enhanced.

In the paper by Timmermann et al. (2005), the response in ENSO variability to the weakening of the Atlantic THC

is through the oceanic process (Kelvin wave) that induces a symmetric response in the tropical Pacific across the Equator. However, the impact of the oceanic waves is very weak as compared to the atmospheric response, and the more recent study by Timmermann et al. (2007) confirms that the response has opposite sign across the Equator in the tropical Pacific due to the atmospheric process.

In summary, the global-scale atmospheric transport becomes stronger in following an abrupt climate change (Perturbed case). One can say that the Perturbed climate is similar to the DJF climate in the Control case: for both DJF and JJA seasons there is cooling in the Northern Hemisphere and warming over the Southern Hemisphere which enhances the northward heat transport.

Possible extensions of this study could include taking into account convection and more accurate modeling of the mixing barriers. Applications of this work include the analysis of the transport of atmospheric pollutants. Since many atmospheric pollutants can be treated as passively transported by the atmospheric flow, this study helps to understand how the atmosphere of the past and potential future climate would transport atmospheric constituents and pollutants. It can have important implications for atmospheric chemistry: the quantitative measure of the

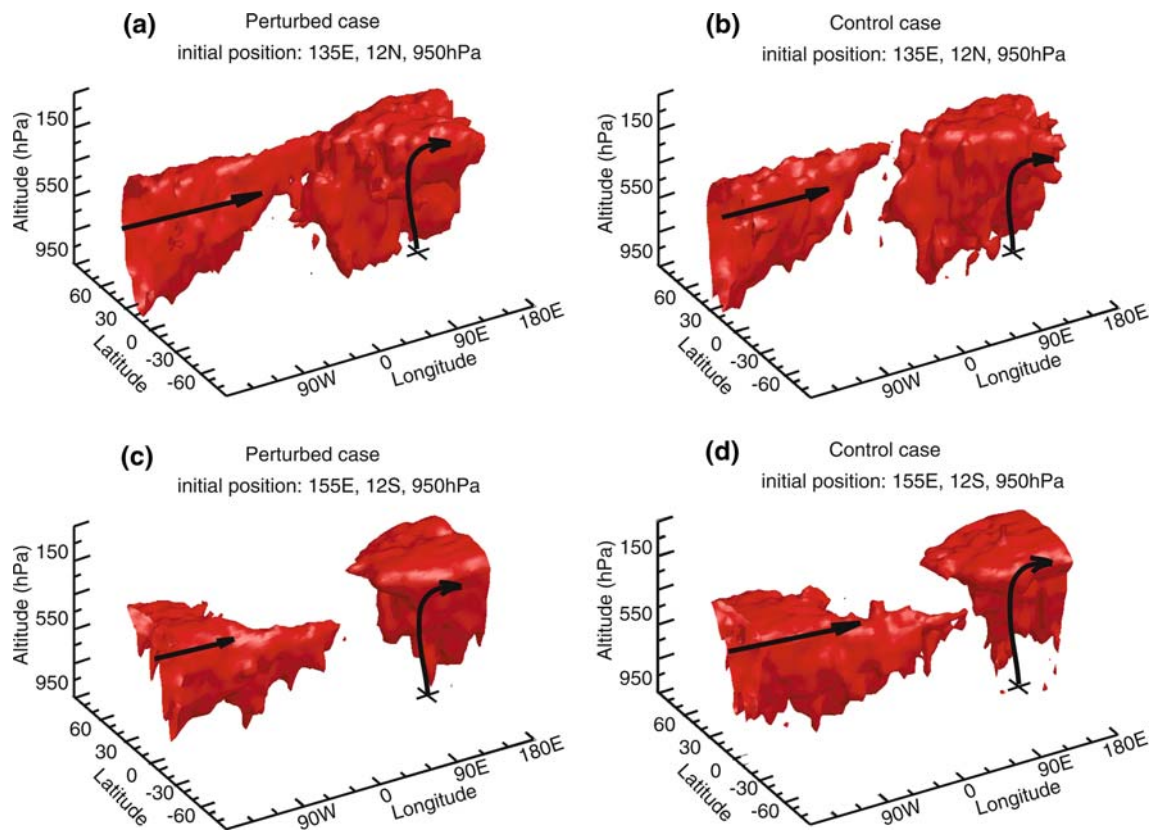


**Fig. 8** 3-D Green's functions calculated for the Perturbed (left panel) and Control (right panel) cases. The initial position of parcels is indicated by a cross and numbers in each figure. Black arrows

indicate the preferential direction of transport. Thicker arrows reflect stronger upward and eastward transport. All distributions are plotted for DJF 20 days after the parcels' initial release

global-scale transport of trace gases in the troposphere is very important for understanding its photochemical activity. Recent studies showed that the upper troposphere is more photochemically active than previously thought due to the convective transport of radical precursors (e.g., Mari et al. 2004 and references therein). Capitalizing on our current and previous studies (Erukhimova and Bowman 2006), we will discuss the convective transport of chemical tracers under the abrupt climate change scenario in future work.

## References

- Altabet MA, Higginson MJ, Murray DW (2002) The effect of millennial-scale changes in Arabian Sea denitrification on atmospheric CO<sub>2</sub>. *Nature* 415:159–162
- Austin J, Tuck AF (1985) The calculation of stratospheric air parcel trajectories using satellite data. *Quart J Roy Meteor Soc* 111:279–307
- Bowman KP (1993) Large-scale isentropic mixing properties of the Antarctic polar vortex from analyzed winds. *J Geophys Res* 98:23013–23027
- Bowman KP (1996) Rossby wave phase speeds and mixing barriers in the stratosphere. Part I: Observations. *J Atmos Sci* 53:905–916
- Bowman KP (2006) Transport of carbon monoxide from the tropics to extratropics. *J Geophys Res* 111:D02107. doi:10.1029/2005JD00617
- Bowman KP, Carrie GD (2002) The mean-meridional transport circulation of the troposphere in an idealized GCM. *J Atmos Sci* 59:1502–1514
- Bowman KP, Erukhimova TL (2004) Comparison of Global-Scale Lagrangian Transport Properties of the NCEP reanalysis and CCM3. *J Clim* 17:1135–1146
- Broccoli AJ, Dahl KA, Stouffer RJ (2006) The Response of the ITCZ to Northern Hemisphere cooling. *Geophys Res Lett* 33:L01702. doi:10.1029/2005GL024546
- Bryden HL, Longworth HR, Cunningham SA (2005) Slowing of the Atlantic meridional overturning circulation at ±25°N. *Nature* 438:655–657
- Chen P (1994) The permeability of the Antarctic vortex edge. *J Geophys Res* 99:20563–20571
- Cheng W, Bitz CM, Chiang JCH (2007) Adjustment of the global climate to an abrupt slowdown of the Atlantic meridional overturning circulation. In: Schmittner, Chiang, Hemming (eds) *In press for Ocean Circulation: Mechanisms and Impacts* (AGU Monograph). doi:10.1029/173GM19
- Chiang JCH, Biasutti M, Battisti DC (2003) Sensitivity of the Atlantic intertropical convergence zone to last glacial maximum boundary conditions. *Paleoceanography* 18. doi:10.1029/2003PA000916
- Dahl KA, Broccoli AJ, Stouffer R (2005) Assessing the role of North Atlantic freshwater forcing in millennial scale climate variability: a tropical Atlantic perspective. *Clim Dyn* 24:325–346. doi:10.1007/s00382-004-0499-5

- Delworth TL et al (2006) GFDLs CM2 global coupled climate models Part 1: Formulation and simulation characteristics. *J Clim* 19:643–674
- Erukhimova TL, Bowman KP (2006) Role of convection in global-scale transport in the troposphere. *J Geophys Res* 111:D03105. doi:10.1029/2005JD006006
- Hall TM, Plumb RA (1994) Age as a diagnostic of stratospheric transport. *J Geophys Res* 99:1059–1070
- Holzer M (1999) Analysis of passive tracer transport as modeled by an atmospheric general circulation model. *J Clim* 12:1659–1684
- Holzer M, Boer GJ (2001) Simulated changes in atmospheric transport climate. *J Clim* 14:4398–4420
- Holzer M, Hall TM (2000) Transit-time and tracer-age distributions in geophysical flows. *J Atmos Sci* 57:3539–3558
- Hsu CPF (1980) Air parcel motions during a numerically simulated sudden stratospheric warming. *J Atmos Sci* 37:2768–2792
- Kida H (1983) General circulation of air parcels and transport characteristics derived from a hemispheric GCM. Part 2. Very long-term motions of air parcels in the troposphere and stratosphere. *J Meteor Soc Japan* 61:510–522
- Koutavas A, Lynch-Stieglitz J, Marchitto TM Jr., Sachs JP (2002) El-Niño-like pattern in Ice age tropical Pacific sea surface temperature. *Science* 297:226–230
- Mari C et al (2004) Export of Asian pollution during two cold front episodes of the TRACE-P experiment. *J Geophys Res* 109:D15S17. doi:10.1029/2003JD004307
- Matsuno T (1980) Lagrangian motion of air parcels in the stratosphere in the presence of planetary waves. *Pure Appl Geophys* 118:189–216
- Peterson LC, Haug GH, Hughen KA, Rohl U (2000) Rapid changes in the hydrologic cycle of the tropical Atlantic during the last glacial. *Science* 290:1947–1950
- Pierce RB, Fairlie TDA (1993) Chaotic advection in the stratosphere: Implications for the dispersal of chemically perturbed air from the polar vortex. *J Geophys Res* 98:18589–18595
- Pierrehumbert RT, Yang H (1993) Global chaotic mixing on isentropic surfaces. *J Atmos Sci* 50:2462–2480
- Schoeberl MR, Sparcling LC, Newman PA, Rosenberg JE (1992) The structure of the polar vortex. *J Geophys Res* 97:7859–7882
- Stouffer RJ, Dixon KW, Spelman MJ, Hurlin W, Yin J, Gregory JM, Weaver AJ, Eby M, Flato GM, Robitaille DY, Hasumi H, Oka A, Hu A, Jungclaus JH, Kamenkovich IV, Levermann A, Montoya M, Murakami S, Nawrath S, Peltier WR, Vettoretti G, Sokolov A, Weber SL (2006) Investigating the causes of the response of the thermohaline circulation to past and future climate changes. *J Clim* 19:1365–1387
- Sutton RT, Maclean H, Swinbank R, O'Neill A, Taylor FW (1994) High-resolution stratospheric tracer fields estimated from satellite observation using Lagrangian trajectory calculations. *J Atmos Sci* 51:2995–3005
- Timmermann A, An S-I, Krebs U, Goosse H (2005) ENSO suppression due to weakening of the North Atlantic thermohaline circulation. *J Clim* 18:3122–3139
- Timmermann A, Okumura Y, An S-I, Clement A, Dong B, Guilyardi E, Hu A, Jungclaus J, Krebs U, Renold M, Stocker TF, Stouffer RJ, Sutton R, Xie S-P, Yin J (2007) The influence of shutdown of the Atlantic meridional overturning circulation on ENSO. *J Clim* 20:4899–4919
- Vellinga M, Wood RA (2002) Global climate impacts of a collapse of the Atlantic thermohaline circulation. *Clim Change* 54:251–267
- Wang YJ, Cheng H, Edwards RL, An ZS, Wu JY, Shen C-C, Dorale JA (2001) A high-resolution absolute-dated late Pleistocene monsoon record from Hulu Cave, China. *Science* 294:2345–2348
- Wang XF, Auler AS, Edwards RL, Cheng H, Cristall PS, Smart PL, Richards DA, Shen CC (2004) Wet periods in northeastern Brazil over the past 210 kyr linked to distant climate anomalies. *Nature* 432:740–743
- Zhang R, Delworth TL (2005) Simulated tropical response to a substantial weakening of the Atlantic thermohaline circulation. *J Clim* 18:1853–1860